ADVANCED MATERIALS
www.advmat.de

Room-Temperature Spin Transport in C_{60}-Based Spin Valves

*Marco Gobbi, Federico Golmar, Roger Llopis, Fèlix Casanova, and Luis E. Hueso**

Spintronics, or the possibility of performing electronics with the spin of the electron, has been fundamental for the exponential growth of digital data storage which has occurred in the last decades. Indeed, hard-disk drives read-heads are the maximum exponent of what is currently being called first-generation spintronic devices. Current read-heads, although technologically very complex, are scientifically based simply on the tunnel magnetoresistance effect (TMR; magnetoresistance being the change in electrical resistance of a device under the application of an external magnetic field). A tunnel magnetoresistive vertical spin valve is composed of two ferromagnetic layers separated by a thin (around 1 nm) insulating layer, and the resistance of the structure can be switched between two different values upon the application of a magnetic field capable of rotating the magnetization vector of the ferromagnetic layers from parallel to antiparallel.[1] For the eventual success of a second-generation of spintronic devices, more complex mechanisms than the nanometre-distance spin transport in metallic or insulating materials have to be obtained. In particular, coherent spin transport at distances above a few nm and spin manipulation are unavoidable requirements for the production of sophisticated prototypes of, for example, spin transistors or spin light-emitting diodes.[2,3] Organic semiconductors (OS) have emerged as promising materials for advanced spintronics applications. Their spin relaxation mechanisms, mainly represented by spin orbit interaction and hyperfine interaction with protons,[4] are very small, and long spin lifetimes have been consistently detected.[5] Moreover, in spite of the relatively low carrier mobility of these materials, organic vertical spin valves with semiconducting channels thicker than 100 nm have been demonstrated.[6–11] In parallel, OS ultrathin layers perform successfully as spin tunnel junctions, and extremely high (>300%) magnetoresistance (MR) values have been obtained at low temperatures.[12] Regarding possible applications of spin transport in OS, a basic operational requirement is the room temperature (RT) operation of the devices. So far, only organic spin tunnel junctions have shown any significant MR effect at RT.[13–17] By contrast, most devices employing thicker organic layer (>15 nm) show a clear decay of the MR well below RT.[6–11,18]

M. Gobbi, Dr. F. Golmar, R. Llopis, Prof. F. Casanova, Prof. L. E. Hueso
CIC nanoGUNE Consolider
Tolosa Hiribidea 76, 20018 Donostia–San Sebastian, Spain
E-mail: l.hueso@nanogune.eu
Prof. F. Casanova, Prof. L. E. Hueso
IKERBASQUE, Basque Foundation for Science, 48011 Bilbao, Spain
Dr. F. Golmar
on leave from I.N.T.I.–CONICET, Av. Gral. Paz 5445
Ed. 42, B1650JKA, San Martín, Bs As, Argentina

DOI: 10.1002/adma.201004672

In this work, we present significant RT MR values (in excess of 5%) on C_{60}-based vertical spin valves for different thickness of the C_{60} interlayer (from 5 nm to 28 nm) up to high applied biases (~1 V), demonstrating coherent spin transport through C_{60} molecules. We also show that transport of spin-polarized electrons is in agreement with a multi-step tunnelling regime.

C_{60}, the first discovered fullerene, was chosen considering its several properties that make it ideal for organic spintronic devices. Firstly, C_{60} molecules can be sublimated in ultra-high vacuum (UHV) and can, therefore, be cleanly sandwiched between ferromagnetic metallic thin films and integrated in vertical devices. Secondly, C_{60} molecules are very robust and can sustain the top metallic electrode without being damaged, unlike other organic materials. Thirdly, hyperfine interaction is supposed to be very weak in fullerenes due to the absence of polarized hydrogen nuclei and because of the small natural abundance of the ^{13}C nuclear spin (below 2%).[11] Finally, C_{60} lowest unoccupied molecular orbital (LUMO) is quite well matched with the Fermi energy of common ferromagnetic metals, such as Cobalt or Permalloy ($Fe_{80}Ni_{20}$, Py), making possible a relatively easy current injection from magnetic electrodes while keeping a moderate energy injection barrier (see **Figure 1**a). [19]

$Co/AlO_x/C_{60}/Py$ vertical spin valves were fabricated in-situ in a UHV dual chamber evaporator (base pressure < 10^{-9} mbar). The spin valves cross-bar geometry was obtained by deposition through shadow masks on Si/SiO_2 (150 nm) substrates. Junction areas range from 200×200 m to 500×200 m. In every chip, five 15-nm-thick Co lines were deposited as bottom electrodes. A thin Al layer (0.9 nm) was deposited on top of them and was oxygen-plasma oxidized in-situ. A C_{60} layer, with thickness between 5 and 28 nm, was also evaporated through a shadow mask which was designed in such a way that the fullerene only covered 3 of the 5 bottom lines. Hence, two Co electrodes were left only with the thin AlO_x layer and are used as reference junctions. Finally, the sample was completed with the evaporation of a 20-nm-thick Py top electrode (see Figure 1b and 1c for a sketch of the devices).

Structural and morphological quality, together with the thicknesses of the different layers that compose the spin valves, were characterized using X-ray reflectivity (XRR) and atomic force microscopy (AFM). XRR data show clear interference oscillations caused by the exceptional long-range homogeneity of the thin films. This result was expected for the Co bottom electrode film (see **Figure 2**a) as it had been grown on a very smooth SiO_2 surface. However, even a C_{60}/Py bilayer shows a clear interference pattern with double periodicity created by the extra interface between the C_{60} and the metal film (see Figure 2b). Surface roughness was measured directly with AFM and by fitting XRR data, both techniques showing a good agreement. The bottom Co/AlO_x electrode has a rms roughness (r) of 0.2 nm

© 2011 WILEY-VCH Verlag GmbH & Co. KGaA, Weinheim

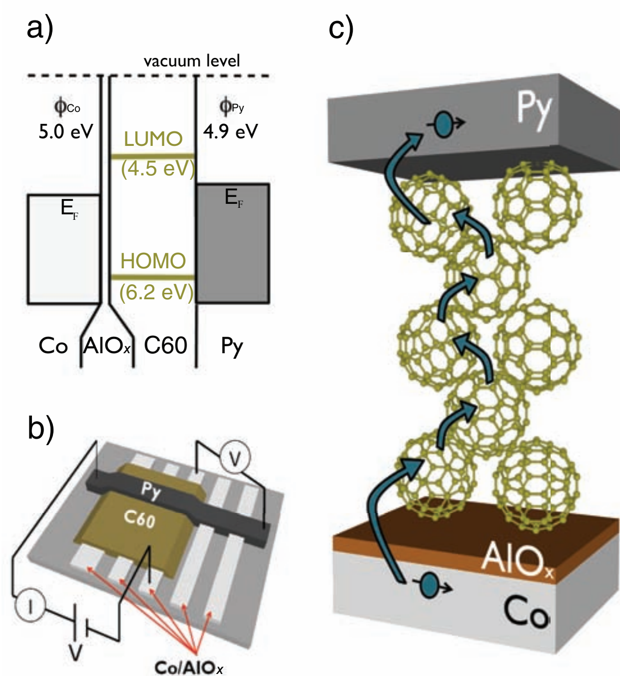

Figure 1. (a) Rigid energy band diagram for the Co/AlO_x/C_{60}/Py stack. (b) Schematic of our spin valve device. Only 3 of the 5 bottom Co electrodes are covered with C_{60}, in such a way that in every chip there are 3 organic junctions and 2 reference junctions with only an AlO_x layer. (c) Ideal representation of a cross-section of our C_{60}-based spin valves.

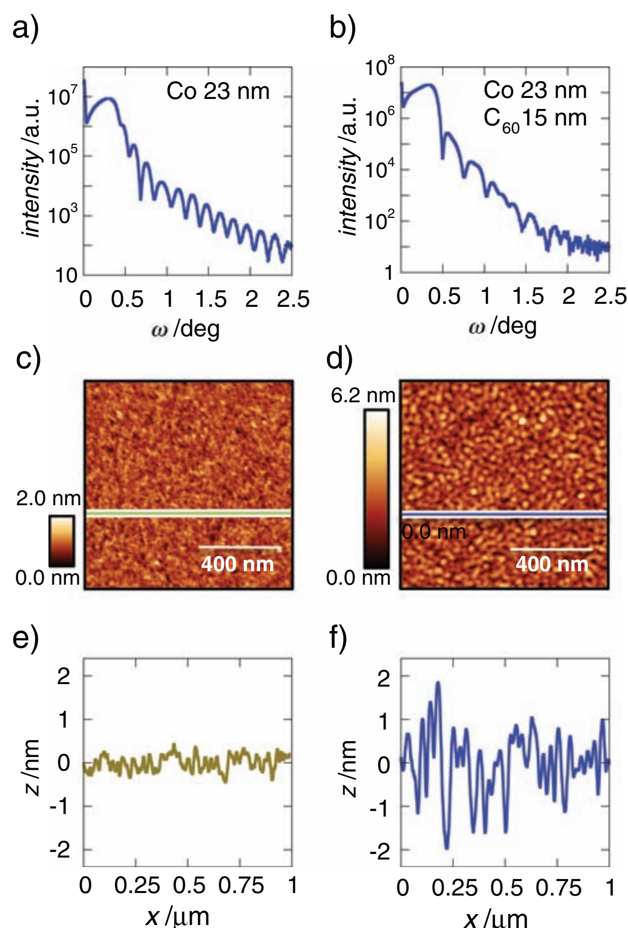

Figure 2. (a) X-Ray reflectivity data for a Co(23 nm)/AlO_x(1 nm) bilayer and (b) for a C_{60}(15 nm)/Py (17 nm) bilayer. Several interference peaks are visible in both measurements, characteristic of extremely small long-range roughness. (c), (d) Atomic force microscopy (AFM) images of, respectively, the Co/AlO_x bottom electrode and the Py top electrode grown on the complete Co/AlO_x/C_{60}/stack (note the different *z*-scale). The profiles along the lines highlighted in (c) and (d) are shown in (e) and (f), respectively. The top Py contact is rougher than the bottom Co layer, as it reflects the surface of the C_{60} layer underneath.

(Figure 2c,e). The subsequent C_{60} layer shows a rms roughness $r = 0.7$ nm, independently of its thickness and consistent with a molecular size of around 1 nm. Finally, the top Py layer follows the morphology of the C_{60} layer, resulting in $r = 0.7$ nm (see Figure 2d,f).

In previous studies of organic tunnel junctions a fully-optimized inorganic tunnel barrier was inserted between the bottom ferromagnetic electrode and the OS.[13–17] As a consequence, it is sometimes difficult to separate the effect of the inorganic from that of the organic barrier. Nevertheless, the AlO_x layer is needed for its important role in isolating the molecules from the Co underlayer, since Co is well known for being very reactive with different organic molecules.[20] In our case we employed a very thin AlO_x layer which does not form a tunnel barrier. In every chip the reference junctions without C_{60} show linear *I–V* curves, with a RT resistance area (RA) product around 2×10^{-4} Ω cm^2 which decreases when lowering the temperature as in a normal metal. Furthermore, no TMR was observed in any case, but only anisotropic MR coming from the metallic electrodes (not shown). The choice of a “leaky” AlO_x film, rather than a fully functional tunnel barrier, ensures that in the hybrid ferromagnetic-organic junctions we are actually measuring the electronic properties of the C_{60} molecules, since any conductive path across the molecular layer (so-called pin-holes) would immediately eliminate any TMR effect.

We move now to the electronic transport properties of the vertical spin valves, in which C_{60} is sandwiched between the ferromagnetic electrodes. For C_{60} thicknesses below 10 nm, the RT current-voltage (*I–V*) curves are non-linear and symmetric, similar to the representative curve of **Figure 3**a. In this thickness range the resistance at low voltage (10 mV) increases around 40% when lowering the temperature down to 80 K (Figure 3c). The *I–V* traces become progressively more asymmetric as the C_{60} thickness is increased (see Figure 3b for a representative sample). Above a thickness of 20 nm, the low-bias resistance (measured at 10 mV) increases typically 400% when lowering the temperature down to 200 K, keeping below that temperature an almost constant value (Figure 3d). The temperature behaviour of the resistance does not follow in any case a simple thermally activated law. We will show below that this temperature behaviour is compatible with the conductivity dominated by quantum-mechanical tunnelling from molecule to molecule.

The resistance area product of all our samples (measured at 10 mV) increases exponentially with C_{60} thickness in the range

© 2011 WILEY-VCH Verlag GmbH & Co. KGaA, Weinheim

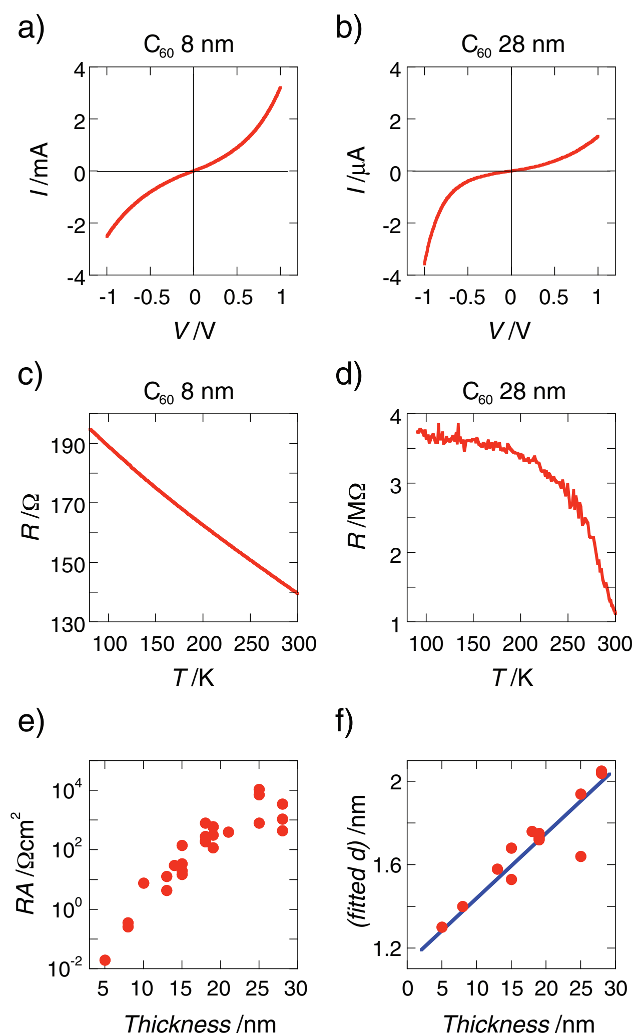

Figure 3. (a), (b) Room temperature Current-voltage (*I–V*) traces for samples with 8 and 28 nm of C_{60} respectively. (c), (d) Temperature dependence of the resistance measured at 10 mV for samples with 8 and 28 nm C_{60} thicknesses. (e) Room temperature low-bias resistance vs thickness of C_{60} layer. (f) Tunnel barrier thicknesses obtained by fitting the room temperature *I–V* traces with the Simmons equation (see text) as a function of the nominal C_{60} thickness.

from 5 to 28 nm, spanning almost six orders of magnitude (Figure 3e). An exponential increase of the resistance with the interlayer thickness is expected in a quantum mechanical tunnelling framework. For example, the standard Simmons model for coherent tunnelling[21] is based on the approximation that the probability (D) for an electron to penetrate a potential barrier can be expressed as:

$$D \propto e^{-\frac{\sqrt{m\phi}}{h}d} \quad (1)$$

where d is the barrier thickness, ϕ is the mean barrier height above the Fermi level of the negatively biased electrode, m is the electron mass and h is the Planck's constant.

We fitted 14 individual room temperature *I–V* traces at positive bias, corresponding to different C_{60} thicknesses, to the equation proposed by Simmons.[21] From each fit we can extract both ϕ and d of the tunnel barrier. The barrier height ϕ is fairly constant for all thicknesses, with a value averaged over the 14 *I–V* traces of 2.4 ± 0.36 eV. The effective thickness d is always much smaller than the nominal C_{60} thickness, but a linear relation is present between these quantities (Figure 3f). For the interpretation of this linear dependence, we follow a simple multistep tunnelling model.[22] In this model the electrons are injected from the metal through an interface barrier into the first molecular layer, and then they undergo a number of tunnelling steps from molecule to molecule until they reach the second electrode. Hence, the probability of an electron crossing the whole molecular layer will be the product of the probabilities of each tunnelling event:

$$D \propto t_{\mathrm{i}} \times \prod_{\mathrm{n}} t_{\mathrm{n}} \quad (2)$$

where t_i is the transmission coefficient of the interface between the metal and the organic material and accounts for both the presence of "leaky" AlO_x layer and for the mismatch between the LUMO and the electrode Fermi energy. n is the number of molecules that an electron encounters in its path from the first to the second electrode, whereas t_n represents the transmission coefficient of each tunnelling process between adjacent molecules and can be expressed following Equation (1), so that:

$$D \propto e^{-a_{\mathrm{i}}} \times \prod_{\mathrm{n}} e^{-a_{\mathrm{n}}} = e^{-(a_{\mathrm{i}} + n a_{\mathrm{n}})} \quad (3)$$

where a_n is the effective intermolecular distance and a_i is the thickness of the interfacial barrier. This model allows us to separate the contribution to the resistance of the interface from that of the molecular layer. By comparing Equations (1) and (3), we can deduct that in this model the relevant tunnelling thickness is not the whole C_{60} thickness, but rather the effective thickness $d = a_i + na_n$, i.e., the sum of an interfacial contribution plus each intermolecular distance multiplied by the number n of molecules in the electron path. n can be estimated as $n = 2x/c$, where x is the actual C_{60} thickness, and $c = 14.17$ Å is the lattice parameter of the C_{60} face-centered cubic (fcc) crystal structure.[23] The factor 2 accounts for the fact that electrons encounter two molecules in every single fcc cell (Figure 1c). Since n increases linearly with the layer thickness x, also d should scale linearly with the actual C_{60} layer thickness, in good agreement with our finding obtained fitting the *I–V* traces to the Simmons equation (Figure 3f). In this same figure 3f the interception at zero C_{60} thickness is 1.15 nm, which represents the thickness of the interfacial barrier a_i. The value of the effective intermolecular distance a_n can be simply obtained as $a_n = (d - a_i)/n = 0.2$ Å. This very small effective intermolecular distance can be explained considering that at RT the tunnel electron might access empty states, which would have energy higher than LUMO and a different charge density distribution in the molecule. At a certain empty state, the charge density may be located very close to its neighbor molecule.

Similar thickness dependence of the resistance was observed in early stages of the research on fullerene samples, although a simpler explanation was then provided.[24] Here, our simple model is capable of explaining the observed temperature

© 2011 WILEY-VCH Verlag GmbH & Co. KGaA, Weinheim

dependence of the resistance as well (see above). Tunnelling processes present only a weak temperature dependence, deviating from a thermally activated behaviour which is observed in organic bulk-dominated samples.

We should highlight that each tunnelling process is inherently spin-conserving; hence, our interpretation of the electronic transport between molecules, together with the very small intramolecular spin relaxation mechanisms, suggests that coherent spin transport over relatively long distances should be observed in our C_{60}-based spin valves.

Accordingly, and very noticeably, MR signals are recorded at RT for every C_{60} thickness sampled (up to 28 nm). This constitutes a very relevant point, since, as explained above, substantial MR (>1%) at RT has been typically ascribed only to organic tunnel junctions with ultra-thin molecular layers.[6–18] **Figure 4**a represents a typical RT MR curve for samples with C_{60} thickness below 15 nm. In this thickness range MR values as high as 10% are measured at RT and do not increase significantly at 80 K. The rounded shape of the MR and the low coercive fields suggest that the antiparallel state is not well stabilized, most likely due to the small magnetic shape anisotropy created by our cross-bar junction configuration and a possible magnetic coupling between electrodes at such C_{60} thickness. For organic thicknesses above 15 nm, several steps are always observed in the transition from the antiparallel to the parallel state (Figure 4b). These steps are most probably related to an increase in magnetic pinning sites as a consequence of increasing surface roughness with thickness. The pinning sites alter the intrinsic coercive field of the magnetic layers, giving rise to pseudo-stochastic behaviour in the MR. [25,26]

In any case, and irrespectively of the micromagnetic details of the magnetization reversal process in the electrodes, significant MR (up to 5.5%) is measured at RT in the 28 nm sample. MR values become even larger (≈8.5%) at lower temperatures (80 K). These results compare very positively with the data available in the literature in two different aspects: on one hand, RT MR is usually negligible in samples whose electrodes are highly polarized magnetic oxides (such as manganites). On the other hand, we report RT MR values for thicknesses at least one order of magnitude higher than for samples composed of 3d-ferromagnetic metals and of such prototypical spin transport organic semiconductors as Alq_3. We believe the improved device performance presented in this manuscript is intrinsically related to the superior spin transport properties of the C_{60} molecular interlayer.[13–15] Considering the theoretical model presented above, we expect significant MR values for C_{60}-based hybrid spin valves up to an approximate thickness of 100 nm.

As relevant as the room temperature MR values for thick C_{60} samples is the voltage dependence of that MR (see Figure 3c for a typical curve measured from the sample with 18 nm of C_{60}). At 80 K the MR at low bias reaches 13%, and at a high bias of –1 V the MR is still 0.9%. The slow decay of the MR with applied bias is important since the overall output current increases simultaneously with bias, and relatively large current values are needed for possible applications of spin devices, such as long distance information transport.[27]

In conclusion, we have obtained spin coherent transport in fullerenes at room temperature, as observed from the large values (>5%) of RT MR in relatively thick (>25 nm) fullerene-based spin valves. To interpret our experimental results we present a multi-step tunnelling model capable of explaining both electronic and spin coherent transport in our samples. We believe that both the large MR values and the small decrease of this MR with applied bias are related to the robust intrinsic properties of fullerenes for spin transport. Therefore we expect that many more spin fullerene-based hybrid devices will follow from this report, from ultra-thick (>100 nm) spin valves to the development of more advanced organic spintronics devices, such as the organic spin transistor.

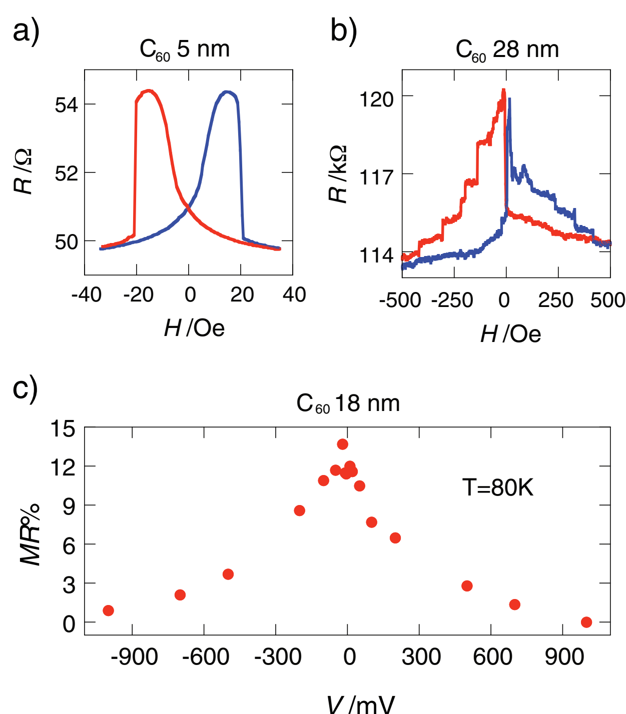

Figure 4. (a), (b) Room temperature magnetoresistance in samples with 5 and 28 nm thickness of C_{60}, respectively. MR values of 9% and 5.5% are measured. The two traces are typical for thin (<10 nm) and thick (>15 nm) C_{60} layers. (c) Bias voltage dependence of the MR for the sample with 18 nm of C_{60} thickness measured at 80 K.

Experimental Section

$Co/AlO_x/C_{60}/Py$ vertical spin valves were fabricated in-situ in a UHV dual chamber evaporator (base pressure < 10^{-9} mbar). Metals were e-beam evaporated in one of the chambers at a rate of 0.1 nm/s, while C_{60} was evaporated in the second one from a Knudsen cell at a rate of 1 nm/min. Metals were 99.95% purity (Lesker), while C_{60} was triple sublimed quality (99.9%) (Sigma Aldrich) and used without further purification. X-ray reflectivity was performed in an X'Pert Panalytical system. Atomic force microscopy images were recorded in tapping mode with a conventional Agilent AFM. Electrical characterization was performed under vacuum in a magnetic-field-equipped variable-temperature probe station (Lakeshore) after the samples had been exposed to air for approximately 1 minute. We should highlight that the conductivity of our C_{60}-based junctions decreases continuously if the samples are not kept under vacuum. This is a well-known effect in fullerenes,[24] since oxygen diffused into the organic acts as a very efficient electron trap. This time relaxation of the conductivity proves indirectly that the carriers

© 2011 WILEY-VCH Verlag GmbH & Co. KGaA, Weinheim

are flowing across the organic materials and that pinholes or metallic conductive paths are absent between the metallic electrodes. A Keithley 4200 semiconductor analyzer system was used to record current (*I*)–voltage (*V*) and magnetoresistance curves.

Acknowledgements

The authors acknowledge financial support from Spanish MICINN project MAT2009-08494 and from the European Comission Marie Curie grant PIRG06-GA-2009-256470.

Received: December 20, 2010
Published online:

[1] J. S. Moodera, L. R. Kinder, T. M. Wong, R. Meservey, *Phys. Rev. Lett.* **1995**, *74*, 3273.
[2] I. Zutic, J. Fabian, S. das Sarma, *Rev. Mod. Phys.* **2003**, *76*, 323.
[3] A. Fert, *Rev. Mod. Phys.* **2008**, *80*, 1517.
[4] T. D. Nguyen, G. Hukic-Markosian, F. Wang, L. Wojcik, X. Li, E. Ehrenfreund, Z. V. Vardeny, *Nat. Mater.* **2010**, *9*, 345.
[5] D. R. McCamey, H. A. Seipel, S. Y. Paik, M. J. Walter, N. J. Borys, J. M. Lupton, C. Boehme, *Nat. Mater.* **2008**, *7*, 723.
[6] V. A. Dediu, L. E. Hueso, I. Bergenti, C. Taliani, *Nat. Mater.* **2009**, *8*, 707.
[7] Z. H. Xiong, D. Wu, Z. Valy Vardeny, J. Shi, *Nature* **2004**, *427*, 821.
[8] L. E. Hueso, I. Bergenti, A. Riminucci, Y. Zhan, V. Dediu, *Adv. Mater.* **2007**, *19*, 2639.
[9] V. Dediu, L. E. Hueso, I. Bergenti, A. Riminucci, F. Borgatti, P. Graziosi, C. Newby, F. Casoli, M. P. De Jong, C. Taliani, Y. Zhan, *Phys. Rev. B* **2008**, *78*, 115203.
[10] Y. Liu, S. M. Watson, T. Lee, J. M. Gorham, H. E. Katz, J. A. Borchers, H. D. Fairbrother, D. H. Reich, *Phys. Rev. B* **2009**, *79*, 075312.
[11] F. Wang, Z. V. Vardeny, *Synth. Met.* **2010**, *160*, 210.
[12] C. Barraud, P. Seneor, R. Mattana, S. Fusil, K. Bouzehouane, C. Deranlot, P. Graziosi, L. Hueso, I. Bergenti, V. Dediu, F. Petroff, A. Fert, *Nat. Phys.* **2010**, *6*, 615.
[13] T. S. Santos, J. S. Lee, P. Migdal, I. C. Lekshmi, B. Satpati, J. S. Moodera, *Phys. Rev. Lett.* **2007**, *98*, 016601.
[14] J. H. Shim, K. V. Raman, Y. J. Park, T. S. Santos, G. X. Miao, B. Satpati, J. S. Moodera, *Phys. Rev. Lett.* **2008**, *100*, 226603.
[15] J. J. H. M. Schoonus, P. G. E. Lumens, W. Wagemans, J. T. Kohlhepp, P. A. Bobbert, H. J. M Swagten, B. Koopmans, *Phys. Rev. Lett.* **2009**, *103*, 146601.
[16] G. Szulczewski, H. Tokuc, K. Oguz, J. M. D. Coey, *Appl. Phys. Lett.* **2009**, *95*, 202506.
[17] R. Lin, F. Wang, J. Rybicki, M. Wohlgenannt, K. A. Hutchinson, *Phys. Rev. B* **2010**, *81*, 195214.
[18] Jung-Woo Yoo, H. W. Jang, V. N. Prigodin, C. Kao, C. B. Eom, A. J. Epstein, *Phys. Rev. B* **2009**, *80*, 205207.
[19] S. Braun, W. R. Salanek, M. Fahlman, *Adv. Mater.* **2009**, *21*, 1450.
[20] Y. Zhan, E. Holmström, R. Lizárraga, O. Eriksson, X. Liu, F. Li, E. Carlegrim, S. Stafström, M. Fahlman, *Adv. Mater.* **2010**, *22*, 1626.
[21] J. G. Simmons, *J. Appl. Phys.* **1963**, *34*, 1793.
[22] C. N. Colesniuc, R. R. Biswas, S. A. Hevia, A. V. Balatsky, I. K. Schuller, unpublished.
[23] S. Saito, A. Oshiyama, *Phys. Rev. Lett.* **1991**, *66*, 2637.
[24] A. Hamed, Y. Y. Sun, K. Y. Tao, R. L. Meng, P. H. Hor, *Phys. Rev. B* **1993**, *47*, 10873.
[25] S. Majumdar, R. Laiho, P. Laukkanen, I. J. Väyrynen, H. S. Majumdar, R. Österbacka, *Appl. Phys. Lett.* **2006**, *89*, 122114.
[26] Y. Chan, Y. Hung, C. Wang, Y. Lin, C. Chiu, Y. Lai, H. Chang, C. Lee, Y. J. Hsu, D. H. Wei, *Phys. Rev. Lett.* **2010**, *104*, 177204.
[27] L. E. Hueso, J. M. Pruneda, V. Ferrari, G. Burnell, J. P. Valdes-Herrera, B. D. Simons, P. B. Littlewood, E. Artacho, A. Fert, N. D. Mathur, *Nature* **2007**, *445*, 410.

© 2011 WILEY-VCH Verlag GmbH & Co. KGaA, Weinheim